Activity-induced propulsion and separation of passive chiral particles in liquids

E. Kirkinis ⊙[*] and M. Olvera de la Cruz ⊙
Department of Materials Science & Engineering, Robert R. McCormick School of Engineering
and Applied Science, Northwestern University, Evanston, Illinois 60208, USA
and Center for Computation and Theory of Soft Materials, Northwestern University,
Evanston, Illinois 60208, USA

Recent literature shows that chiral particles driven by vorticity gradients of a base Newtonian liquid can separate only in nonlinear or nonstationary flows. Here, we show that a base Newtonian liquid endowed with rotational degrees of freedom *can* give rise to chiral particle propulsion and separation even in the Stokes flow approximation. We consider active mechanisms generating spatially inhomogeneous vorticity in the base liquid in a channel such as a magnetic torque, a pressure gradient, and a sliding wall. These mechanisms generate regions of spatially inhomogeneous vorticity maintained by the internal angular momentum, propelling the chiral particles according to their handedness. Similar conclusions can be reached when one of the channel walls is replaced by a free surface acted on by surface shear. This behavior is in contrast to the case of standard Newtonian liquids where chiral particle propulsion generated by vorticity gradients is not possible in Stokes flow. This effect can find applications in industry, biology, and medicine.

I. INTRODUCTION

Recent years have seen significant progress in the design and synthesis of active systems [1] executing cooperative functions by the application of external inputs, such as chemical energy [2] and/or electromagnetic fields [3]. Activity has been employed to promote segregation in colloids [4], including those endowed with reduced symmetries, such as chiral particles [5].

Chirality, a ubiquitous property of biomolecules and biomolecular assemblies [6], refers to the lack of inversion symmetry of a particle. This lack of symmetry *in shape* can be employed to propel particles in an active or passive manner [7]. In the active case, propulsion is achieved by coupling the chiral particles' electric dipole moments or magnetization to external electromagnetic fields [8]. In the passive case, chiral particles can be propelled without intrinsic torques by only resorting to their asymmetric shape, cf. Refs. [9,10].

Here, we consider the passive case and a base liquid endowed with rotational degrees of freedom in a channel under either (i) an external magnetic field, (ii) a pressure gradient, (iii) a sliding channel wall, or (iv) a surface shear "wind," when one of the channels walls is replaced by a free surface. Either of these mechanisms imparts energy into the base liquid in the form of internal angular momentum. The generated spatially inhomogeneous regions of vorticity can drive n^- left- and n^+ right-handed chiral particles in a direction perpendicular to the plane of the vortex (cf. Fig. 1) with single chiral particle velocities v_p and $-v_p$, respectively, by taking advantage of their asymmetric shape. Thus, particles of opposite chirality will move in opposite directions. This effect is in contrast
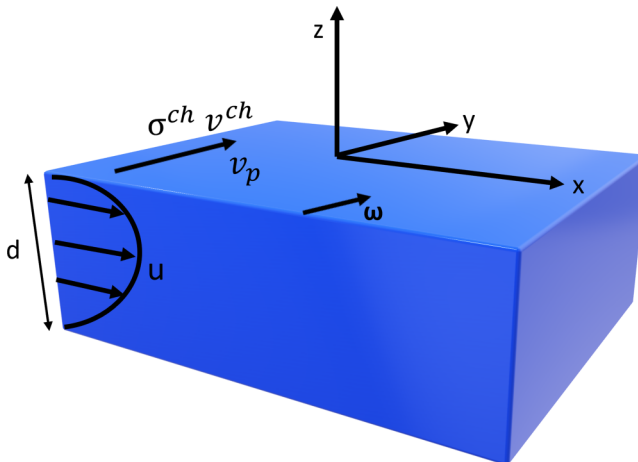
---

*kirkinis@northwestern.edu

FIG. 1. Shear flow $u(z)\hat{\mathbf{x}}$ of a liquid with rotational degrees of freedom [described by the stress and couple-stress tensors Eqs. (3) and (4)] between two rigid plates located at $z = \pm\frac{d}{2}$ (and infinite in the other two directions) gives rise to chiral particle propulsion in the y direction with velocity $v_p(z)\hat{\mathbf{y}}$, a chiral stress $\sigma_{yz}^{\mathrm{ch}}(z)$, and a commensurate (liquid) chiral velocity $v^{\mathrm{ch}}(z)\hat{\mathbf{y}}$. Rotational degrees of freedom are accounted for by the angular velocity $\omega\hat{\mathbf{y}}$ (see the discussion in Sec. II).

to its standard Newtonian liquid counterpart, where propulsion induced by gradients of vorticity is impossible in Stokes flow [10].

Propulsion of an individual particle can be physically justified as follows. The chiral current and thus the individual chiral particle velocity cannot be proportional to liquid vorticity as there should be no chiral current in a rigidly rotating liquid. On the other hand, it *can* be proportional to the difference between vorticity and twice the angular velocity of the rotational degrees of freedom. This effective vorticity rotates the chiral particle which, as a consequence, translates due to its chiral shape.

The motion of the chiral suspension affects the base liquid. Corrections to the Cauchy stress tensor of chiral origin have to be taken into account in a nonracemic mixture. The forces generated are perpendicular to the flow direction. Thus, the chiral suspension also leads to corrections of the liquid velocity directed perpendicularly to the motion of the base flow.

Chirality generates forces on the boundaries by the motion of the chiral particles. In channel flow, the parallel walls experience chiral forces that lie on their plane and are perpendicular to the base flow direction. The two walls experience forces with opposite signs in the pressure-driven flow or the same sign in the two cases of magnetic field and sliding channel walls. We emphasize that although activity may refer to the actuation of matter due to an external magnetic field, the vorticity-generating mechanisms of pressure gradient, sliding of a channel wall, and shearing of a free surface are not concerned with any magnetic properties. We also note that the effect is prominent close to solid boundaries where vorticity gradients are stronger.

In this paper, we attempt to combine logical consistency with completeness. The paper is organized as follows. In Sec. II, we briefly describe the equations of motion for a liquid endowed with rotational degrees of freedom [11]. The liquid can be driven by a rotating magnetic field but it can also be driven by a pressure gradient or a moving boundary. In Sec. III, we review the hydrodynamic equations and constitutive laws for passive chiral particle propulsion and separation as developed in Ref. [10]. This description is then generalized to account for the rotational degrees of freedom of the liquid we consider in this paper. In the subsequent sections, we calculate the force experienced by the liquid from the presence of the chiral particles during their motion, the resulting liquid velocity v^{ch}, and the velocity of an individual chiral particle. The base liquid is driven by

four separate mechanisms. The first mechanism, which gives rise to the most prominent effects, is a magnetic torque, discussed in Sec. IV B. We derive expression and estimate the strength of the observables for a magnetic liquid EMG 900 that has been employed in recent experiments [11]. We report modest estimates for the effects. These can be modified by changing the sizes of the channel, particles, and liquid properties. We repeat the discussion when the effect is driven by the remaining mechanisms: a pressure gradient in Sec. IV C and the practically important case of Couette flow in Sec. IV D. In Sec. IV E, we repeat the foregoing analysis for a liquid layer with a free surface driven by a surface shear wind. We conclude this paper in Sec. V with a discussion of certain applications to which the above mechanism can be applied.

II. REVIEW OF HYDRODYNAMIC EQUATIONS FOR A BASE LIQUID WITH ROTATIONAL DEGREES OF FREEDOM—NO CHIRAL PARTICLES

In the absence of chiral particles, a liquid with rotational degrees of freedom is characterized by the balance of linear and internal angular momentum that can be expressed in the form [12]

$$\rho D u_i / Dt = \partial_k \sigma_{ik} \quad \text{and} \tag{1}$$

$$I D \omega_i / Dt = \partial_k C_{ik} + N_i + \epsilon_{imk} \sigma_{km}, \quad i, k, m = 1, 2, 3, \tag{2}$$

where D/Dt is the convective derivative, ρ is the fluid density, I the volume density of the grain moment of inertia, u_i is the fluid velocity, ω_i the grain angular velocity, and N_i is the magnetic torque density. As noted in Ref. [12], the last term of the second equation in Eqs. (2) represents the transformation of moment of momentum $\epsilon_{ijk} x_i u_j$ into internal angular momentum only when the stress σ_{ij} has an antisymmetric part. It is this antisymmetric part of the base flow constitutive relation that maintains a spatially inhomogeneous vorticity distribution that gives rise to the chiral particle propulsion considered in this paper. The resulting total stress $\boldsymbol{\sigma}$ is [11]

$$\sigma_{ik} = -p \delta_{ik} + \eta \hat{V}_{ik} + \zeta \hat{W}_{ik} + \hat{T}_{ik}, \tag{3}$$

where $\hat{V}_{ik} = \partial_k u_i + \partial_i u_k$ is twice the rate-of-strain tensor, $\hat{W}_{ik} = \partial_k u_i - \partial_i u_k - 2\epsilon_{kil}\omega_l$ is a "spin" tensor measuring the imbalance between liquid and particle angular velocity, $\hat{T}_{ik} = (h_i b_k - \frac{1}{2} h_j^2 \delta_{ik})/4\pi$ is the Maxwell stress tensor, and $\boldsymbol{h}$ and $\boldsymbol{b}$ denote the *macroscopic* magnetic field and induction, respectively. Here, the liquid is considered incompressible $\partial_i u_i = 0$, p is the pressure, and η is the liquid (shear) viscosity. The phenomenological coefficient ζ multiplying $\hat{W}$ in Eq. (3) is termed the vortex viscosity in the literature [11,12], ϵ_{ijk} is the alternating pseudotensor, and we employed the Einstein summation convention on repeated indices. $\hat{W}$ has $(\text{curl}\boldsymbol{u})/2 - \boldsymbol{\omega}$ as its axial vector. Thus, whenever $\hat{W}$ is nonvanishing, there is an imbalance between the liquid vorticity and the angular velocity ω (either of the two can be driven by an external source), and thus transfer of energy takes place from rotational to translational degrees of freedom and vice versa. This guarantees that diffusion of vorticity will be maintained in such a flow even in the Stokes regime, as will be discussed below.

Diffusion of internal angular momentum takes place due to couple stresses **C**,

$$C_{ik} = \eta'(\partial_k \omega_i + \partial_i \omega_k) + \zeta' \partial_j \omega_j \delta_{ik}, \tag{4}$$

the suspended particles experience in their rotational motion. Here η' and ζ' are the shear and bulk coefficients of spin viscosity [12]. Therefore, $\partial_j C_{ij}$ in Eqs. (2) is the rate of arrival of internal angular momentum by way of diffusion.

Incorporating the constitutive assumptions Eqs. (3) and (4) into the balance of linear and internal angular momentum Eqs. (1) and (2), we obtain in familiar vector notation

$$\rho[\partial_t \mathbf{u} + \mathbf{u} \cdot \nabla \mathbf{u}] = -\nabla p + 2\zeta \, \text{curl}\boldsymbol{\omega} + (\zeta + \eta)\nabla^2 \mathbf{u}, \tag{5}$$

$$I[\partial_t \boldsymbol{\omega} + \mathbf{u} \cdot \nabla \boldsymbol{\omega}] = \mathbf{N} + 2\zeta(\text{curl}\mathbf{u} - 2\boldsymbol{\omega}) + \eta' \nabla^2 \boldsymbol{\omega}, \tag{6}$$

and $\nabla \cdot \mathbf{u} = 0$ for an incompressible liquid. Here we introduced the condition $\nabla \cdot \boldsymbol{\omega} = 0$, which is automatically satisfied in the context of the geometry employed in this article.

In this paper, we consider no-slip and no-rotation boundary conditions on a solid surface:

$$\mathbf{u} = \mathbf{0} \quad \text{and} \quad \boldsymbol{\omega} = \mathbf{0}. \tag{7}$$

Both can be relaxed. The angular velocity condition can be replaced by various models that have appeared in the literature [11,12]. The no-slip condition may also be relaxed and replaced by wall slip models [13]. It suffices, however, for the purposes of the present paper to employ Eqs. (7) and limit attention to the chirality-related physical effects rather than an exhaustive enumeration of cases related to different boundary conditions satisfied by the base flow. In this paper, we will also consider a liquid with a free flat surface. In this interface, one has to satisfy a shear stress and couple stress condition,

$$[[\mathbf{t}\boldsymbol{\sigma}\mathbf{n}]] = \tau \quad \text{and} \quad [[\mathbf{C}\mathbf{n}]] = \mathbf{0}, \tag{8}$$

where $\mathbf{n}$ and $\mathbf{t}$ denote the unit normal and tangent on the interface, τ is an imposed surface shear wind [14] and the symbol $[[\cdot]]$ denotes the jump of the field across an interface. The second condition in Eqs. (8), satisfied by a liquid with rotational degrees of freedom, was only recently derived by Chaves and Rinaldi [15] and employed in studies of active matter with a free surface [16].

To make analytical progress, we now introduce the following geometry, which, despite its simplicity, displays all relevant features of the effects conveyed in this paper, and which were absent in Ref. [10]. Consider shear flow between two (no-slip) parallel plates (see Fig. 1) located at $z = \pm d/2$, for which the liquid velocity, particle angular velocity, and liquid vorticity become

$$\mathbf{u} = u(z)\hat{\mathbf{x}}, \quad \boldsymbol{\omega} = \omega(z)\hat{\mathbf{y}}, \quad \text{curl}\mathbf{u} = \hat{\mathbf{y}}\partial_z u. \tag{9}$$

This flow pattern can be justified, for instance, by the application of a rotating magnetic field in the $x - z$ plane, which was shown to arise in several theoretical and experimental instances [17].

In the creeping flow approximation, the Navier-Stokes Eqs. (5) and (6) reduce to

$$\hat{\mathbf{x}}: \quad -\partial_x p - 2\zeta \partial_z \omega + (\zeta + \eta)\partial_z^2 u = 0, \tag{10}$$

$$\hat{\mathbf{y}}: \quad 2\zeta(\partial_z u - 2\omega) + \eta'\partial_z^2 \omega + N = 0. \tag{11}$$

We consider a geometry where the lower boundary of the liquid at $y = -d/2$ is an immobile wall (cf. Fig. 3), with no slip and no particle rotation:

$$u = 0, \quad \text{and} \quad \omega = 0, \quad \text{at } z = -\frac{d}{2}. \tag{12}$$

For the upper wall, located at $y = d/2$, we will investigate the following distinct cases:
   (1) Channel with immobile upper wall; then the boundary conditions read $u = \omega = 0$.
   (2) Channel with moving upper wall: $u = U$ and $\omega = 0$.
   (3) Free surface with shear wind of strength τ: $\sigma_{xz} = \tau$ and $\partial_z \omega = 0$ [15] [derived from Eq. (8)].
   The exact forms of the fields u and ω determined by the solution of Eqs. (10) and (11) with the above boundary conditions appear in Appendix B. They were obtained by considering a constant magnetic torque N, as was derived, for instance, by Zahn and Greer [17] by applying a rotating magnetic field to a ferrofluid suspension and by taking the limit $\omega\tau_B \to 0$, where τ_B is the Brownian relaxation time of the grains.

III. THEORY OF CHIRAL PARTICLE PROPULSION AND SEPARATION IN A LIQUID WITH ROTATIONAL DEGREES OF FREEDOM

In this section, we briefly summarize the main equations and constitutive laws derived in Ref. [10] satisfied by chiral particles suspended in a standard Newtonian liquid. We then generalize

them to account for the rotational degrees of freedom and antisymmetric stress tensors of the base liquid employed in the present paper.

Consider a suspension of $n = n^+ + n^-$ chiral particles per unit volume suspended in the base liquid endowed with the rotational degrees of freedom we described in the previous section. n^+ and n^- are the number densities of right- and left-handed particles, respectively.

Concentration, pressure, and temperature gradients will, in general, affect the distribution of particles in a moving liquid with velocity $\mathbf{u}$ according to $\partial_t n + \mathrm{div}(\mathbf{u}n) + \mathrm{div}\mathbf{j} = 0$, where

$$\mathbf{j}(n) = -D\boldsymbol{\nabla}n - n\lambda_T\boldsymbol{\nabla}T - n\lambda_p\boldsymbol{\nabla}p \tag{13}$$

[10,18].

As seen from the Navier-Stokes equations with rotational degrees of freedom, cf. Eqs. (10) and (11), the shear viscosity is represented by $\eta + \zeta$. Thus, the chiral momentum flux density Eq. (6) of Ref. [10] is modified by incorporating the rotational degrees of freedom and acquires the form

$$\sigma_{ij}^{\mathrm{ch}} = (\eta + \zeta)\{n^{\mathrm{ch}}\alpha[\partial_i(\mathrm{curl}\mathbf{u})_j + \partial_j(\mathrm{curl}\mathbf{u})_i] + \alpha_1[(\mathrm{curl}\mathbf{u})_i\partial_j n^{\mathrm{ch}} + (\mathrm{curl}\mathbf{u})_j\partial_i n^{\mathrm{ch}}]\}, \tag{14}$$

where $n^{\mathrm{ch}} = n^+ - n^-$ is the chiral density.

The evolution of the chiral density can also be affected by advection, concentration, pressure, and temperature gradients:

$$\partial_t n^{\mathrm{ch}} + \mathrm{div}(\mathbf{u}n^{\mathrm{ch}}) + \mathrm{div}(\mathbf{j}(n^{\mathrm{ch}}) + \mathbf{j}^{\mathrm{ch}}) = 0. \tag{15}$$

Here, $\mathbf{j}(n^{\mathrm{ch}})$ is the standard current, Eq. (13), with n replaced by n^{ch}, and $\mathbf{j}^{\mathrm{ch}}$ is a new contribution allowed by symmetry:

$$\mathbf{j}^{\mathrm{ch}} = n\beta\nabla^2\mathrm{curl}\mathbf{u}. \tag{16}$$

This current can be understood as the difference between the current of right-handed particles $\mathbf{j}_+$ and left-handed particles $\mathbf{j}_-$:

$$\mathbf{j}^{\mathrm{ch}} = \mathbf{j}_+ - \mathbf{j}_-. \tag{17}$$

Thus, if $\mathbf{j}_\pm = n^\pm v_p^\pm$ where v_p is the single-particle velocity, then Eq. (17) implies Eq. (16) if we identify $v_p^\pm$ with $\pm\beta\nabla^2\mathrm{curl}\mathbf{u}$. This definition also implies that particles of opposite chirality move in opposite directions.

The coefficients α and β in Eqs. (14) and (16) are determined in the low Reynolds number regime by studying the particle motion in the surrounding liquid [19]. They are given by

$$\alpha \sim \alpha_1 \sim \chi R^4 \quad \text{and} \quad \beta \sim \chi R^3, \tag{18}$$

where R is the chiral particle radius and χ is the degree of chirality in the shape of the particles. For simplicity, we consider an incompressible liquid where the right- and left-handed particles are mirror images of each other. The chiral current Eq. (16) is allowed by symmetry and it is present even in racemic mixtures (where $n^{\mathrm{ch}} \equiv 0$).

Now the question that arises is, In which flows are the above chiral current Eq. (16) present? For example, it is known that in Stokes flow, the above chiral current in Eq. (16) does not give rise to chiral particle propulsion, cf. Ref. [10], unless the base flow is nonlinear or nonstationary. This is not the case, however, when rotational degrees of freedom are incorporated in a liquid where they generate and *maintain* regions of inhomogeneous vorticity gradients. From Eqs. (5) and (6), one can derive the vorticity equation:

$$(\zeta + \eta)\nabla^2\mathrm{curl}\mathbf{u} = 2\zeta\nabla^2\boldsymbol{\omega} + \rho(\partial_t\mathrm{curl}\mathbf{u} + \mathrm{curl}(\mathbf{u} \cdot \boldsymbol{\nabla}\mathbf{u})). \tag{19}$$

As is evident from Eq. (19), the term $\nabla^2\mathrm{curl}\mathbf{u}$ exists even in the Stokes flow approximation, as long as the diffusion of internal angular momentum $\sim\nabla^2\boldsymbol{\omega}$ is nonvanishing. Even in the absence of an external torque $\mathbf{N}$, the diffusion of vorticity can be maintained by the imbalance $\boldsymbol{\nabla} \times \mathbf{u} - 2\boldsymbol{\omega}$ of

TABLE I. Definition of observables and parameters.

Quantity	Units	Definition
v_p	cm/s	Individual chiral particle velocity
j^{ch}	cm/s/cm^3	Chiral current
F	dyne cm^{-2}	Chiral particle-induced stress on channel walls
v^{ch}	cm/s	Chiral particle-induced liquid velocity
$l = \sqrt{\frac{\zeta \eta'}{\eta(\eta+\zeta)}}$	cm	Parameter
$k = \sqrt{\frac{4\eta\zeta}{\eta'(\eta+\zeta)}}$	cm^{-1}	Parameter

the rotational degrees of freedom in the basic liquid in the creeping flow approximation (the Stokes regime) that can be driven by a shear flow, see Eq. (6).

When the chiral density n^{ch} is spatially uniform, only the first term of the general expression for the chiral stress in Eq. (14) is in operation. Then, the chiral volume force density $-\partial_j \sigma_{ij}^{\text{ch}} \equiv -n^{\text{ch}}\alpha(\eta + \zeta)\nabla^2 \text{curl}\mathbf{u}_i$, derived from this term, can be generated not only in nonstationary and nonlinear flows but also in creeping (Stokes) flow.

We note that additional terms of orientational origin exist in the chiral current Eq. (16), see Ref. [10], Eq. (8). These terms are subdominant to the one in Eq. (16) and we will not consider them further.

IV. ILLUSTRATIVE EXAMPLES OF CHIRAL PARTICLE PROPULSION IN A MEDIUM ENDOWED WITH ROTATIONAL DEGREES OF FREEDOM

A. Formulation of observables to be calculated

In the sections that follow, we will predominantly be interested in deriving some practically useful observables that we list in Table I. The first observable is the individual chiral particle velocity v_p, which, from Eq. (16), acquires the form (see Fig. 1)

$$\mathbf{v}_p \equiv \frac{\mathbf{j}^{\text{ch}}}{n} = v_p\hat{\mathbf{y}} \sim \chi R^3 \partial_z^3 u(z)\hat{\mathbf{y}}, \qquad (20)$$

(we drop the $\pm$ superscript on v_p) directed perpendicularly to the plane of the basic flow. Second, the stresses imparted on the channel walls by the motion of the chiral suspension,

$$\mathbf{F} \equiv \hat{\mathbf{y}}\sigma_{yz}^{\text{ch}}\big|_{z=\pm d/2} \sim \hat{\mathbf{y}}\chi R(\eta + \zeta)\partial_z^2 u(z)\big|_{z=\pm d/2}, \qquad (21)$$

are also directed perpendicularly to the plane of the basic flow (see Fig. 1), where we assumed that $n^{\text{ch}}R^3 \sim 1$. Third, the motion of the chiral suspension endows the liquid flow with a velocity component v^{ch} perpendicular to the plane of the basic flow (see Fig. 1) and a commensurate chiral angular velocity ω^{ch},

$$\mathbf{u} = u(z)\hat{\mathbf{x}} + v^{\text{ch}}(z)\hat{\mathbf{y}}, \quad \text{and} \quad \boldsymbol{\omega} = \omega^{\text{ch}}(z)\hat{\mathbf{x}} + \omega(z)\hat{\mathbf{y}}, \qquad (22)$$

where the fields with the superscript $^{\text{ch}}$ should be considered as a chirality-induced perturbation superposed on the base flow $u(z)\hat{\mathbf{x}}$ and $\omega(z)\hat{\mathbf{y}}$. Thus, balance Eqs. (1) and (2) must be updated so the Cauchy stress tensor σ_{ij} also contains the chiral stress contribution Eq. (14). This gives rise to two extra equations that must be satisfied by the fields $v^{\text{ch}}(z)$ and $\omega^{\text{ch}}(z)$. They read

$$\hat{\mathbf{y}}: \quad 2\zeta\,\partial_z\omega^{\text{ch}} + (\zeta + \eta)\partial_z^2 v^{\text{ch}} + \chi R(\eta + \zeta)\partial_z^3 u = 0 \qquad (23)$$

and

$$\hat{\mathbf{x}}: \quad 2\zeta(-\partial_z v^{\text{ch}} - 2\omega^{\text{ch}}) + \eta'\partial_z^2\omega^{\text{ch}} = 0, \qquad (24)$$

where the basis vectors $\hat{\mathbf{x}}$ and $\hat{\mathbf{y}}$ denote the physical space direction for the conservation of linear and internal angular momentum, respectively. The last term of the first equation is the contraction of the chiral stress Eq. (14) where u is given by Eq. (B2). Equations (23) and (24) must be accompanied by suitable boundary conditions, which, for the case of a channel correspond to no slip and no rotation:

$$v^{\text{ch}}\left(\pm\frac{d}{2}\right) = \omega^{\text{ch}}\left(\pm\frac{d}{2}\right) = 0. \tag{25}$$

When the upper channel wall at $z = d/2$ is replaced by a free surface, the conditions of zero shear stress $\sigma_{yz} = 0$ and zero couple stress, cf. Eqs. (8), read

$$(\eta + \zeta)\partial_z v^{\text{ch}} + 2\zeta\omega^{\text{ch}} + \chi R(\eta + \zeta)\partial_z^2 u = 0, \quad \text{and} \quad \partial_z\omega^{\text{ch}} = 0, \quad \text{at } z = \frac{d}{2}. \tag{26}$$

Thus, the chiral stress Eq. (14) generated by the motion of a nonracemic suspension also gives rise to new fluid flow behavior. The contributions to the liquid velocity obtained by the solution of Eqs. (23) and (24) subject to the above boundary conditions are, in general, small compared with the unperturbed liquid velocity. Perturbations to the liquid velocity in other directions may also be included, but here we concentrate on demonstrating the effect imparted only on the chiral velocity and angular velocity components.

We need to interpret the character of the formulas Eqs. (20), (21) and (23), (24) for the observables v_p, F, and v^{ch} under spatial inversion. Under spatial inversion, it is clear that $n^{\pm} \to n^{\mp}$. From Eq. (17), it is seen that the chiral current $\mathbf{j}^{\text{ch}}$ does not change sign under spatial inversion. Thus, it is not a true (polar) vector but an axial (pseudo)vector. Thus, all terms in the continuity Eq. (15) change signs. Likewise, we enforce the same rule in Eq. (21) for the chiral stress and thus for the chiral fields v^{ch} and ω^{ch} as well, by solution of Eqs. (23) and (24). In these equations, the sign of χ is, however, also associated with the sign of n^{ch}. If we consider a racemic mixture, we must set $\chi = 0$ in Eqs. (21), (23), and (24) and in associated boundary conditions. These rules provide a clear physical interpretation of the effects and ensures the invariance of Eqs. (23) and (24) under spatial inversion. In what follows, we will adopt the value $\chi = 1$ in the numerical calculations of the effect. Since all effects are linear in χ, the readers can then multiply by the exact value of χ to obtain estimates of the effects with respect to the particles they employ.

The above observables are spatially dependent. In the ensuing sections, we calculate their characteristic values by averaging over the width of the channel, so, for instance, the average particle velocity is

$$\langle v_p \rangle = \frac{1}{d} \int_{-d/2}^{d/2} v_p(z)dz. \tag{27}$$

When the average vanishes, we characterize the strength of the observable by its two-norm, which, for the case of particle velocity, is defined as follows:

$$\|u\|_2 = \sqrt{\frac{1}{d} \int_{-d/2}^{d/2} v_p^2(z)dz}, \tag{28}$$

so it retains correct units.

B. Passive chiral particle propulsion induced by a magnetic torque stirring of the base magnetic liquid

When the base liquid is magnetic, for instance, a ferrofluid (cf. Fig. 2), a magnetic field rotating in the $x - z$ plane, produces a magnetic torque

$$N = N_0 + O(\omega\tau_B) \tag{29}$$

directed along the y axis (see Eq. (34) of Ref. [17], Eq. (48) of Ref. [11], and Eqs. (2.24)– (2.32) of Ref. [20]), in the limit of slow rotation $\omega\tau_B \to 0$, where τ_B is the Brownian relaxation time of
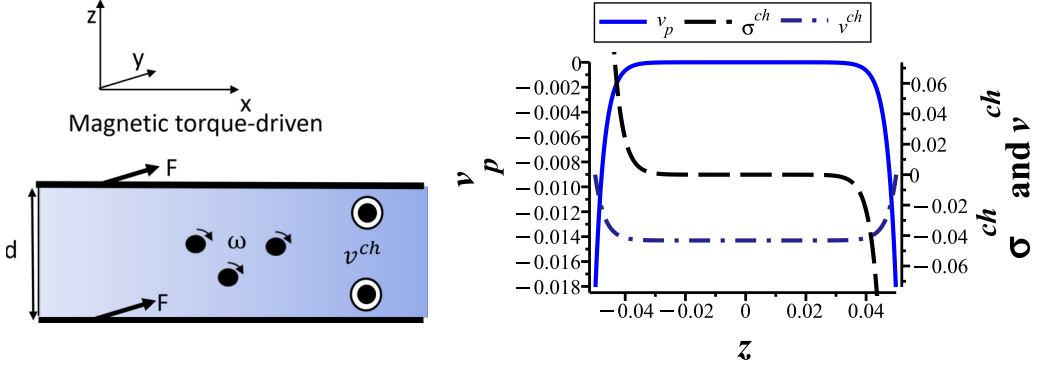
FIG. 2. The magnetic torque-induced flow of a ferrofluid EMG 900_2 (see Table II) in a channel of width d whose dynamics is described by the stress and couple tensors Eqs. (3) and (4) gives rise to passive chiral particle propulsion. (a) Ferromagnetic grains • rotate with angular velocity ω due to a magnetic torque $N = m \times h$, where h is the external rotating magnetic field (see Appendix A). A chiral current j^{ch} [cf. Eq. (16)] is driven by the diffusion of liquid vorticity which in turn is driven by the external torque and the angular velocity imbalance curl$u - 2\omega$. The single chiral particle velocity is denoted by v_p. A chiral stress $F = \sigma_{yz}^{ch}$ perpendicular to the plane of the page [cf. Eq. (14)] applies evenly directed forces F on the channel walls in the y direction. This stress also gives rise to a chiral volume force density $-\partial_z \sigma_{yz}^{ch}$ and a chiral velocity v^{ch} [see Eqs. (23) and (24)] of suspended chiral particles of density $n^{ch} = n^+ - n^-$ directed perpendicularly to the plane of the channel: out of the page ⊙ at the whole expanse of the channel. The right panel shows the spatial distribution of the observables v_p, σ^{ch} and v^{ch} in Gaussian units. The value $\chi = 1$ of the chiral parameter was applied in these plots.

ferroparticles, cf. Eq. (A1). The constant N_0 depends on the frequency and amplitude of the applied field. As shown in Ref. [17], the $O(\omega \tau_B)$ term in Eq. (29) only leads to a renormalization of the coefficient of vortex viscosity ζ. For simplicity, here we only consider the leading order (constant) term N_0 and proceed by dropping the index.

We employ the boundary conditions of no-slip and no-particle rotation at the channel walls

$$u = 0, \quad \text{and} \quad \omega = 0, \quad \text{at } z = \pm\frac{d}{2}, \tag{30}$$

respectively and substitute into Eqs. (10) and (11) to obtain the closed form expression for the fields u and ω that appear in Appendix B.

Defining the dimensional parameters $l = \sqrt{\frac{\zeta \eta'}{\eta(\eta + \zeta)}}$ (measured in cm) and $k = \sqrt{\frac{4\eta\zeta}{\eta'(\eta + \zeta)}}$ (measured in cm^{-1}, cf. Table I), substituting the unperturbed velocity profile $u(z) = -\frac{Nl(d \sinh(kz) - 2\sinh(\frac{kd}{2})z)}{4\zeta(-l \sinh(\frac{kd}{2}) + d \cosh(\frac{kd}{2}))}$ directly into Eq. (20) and averaging over the channel width we obtain the single particle velocity v_p:

$$\langle v_p \rangle \equiv \frac{\langle j^{ch} \rangle}{n} = -\frac{\sinh(\frac{kd}{2}) \chi R^3 l N k^2}{2\zeta(-l \sinh(\frac{kd}{2}) + d \cosh(\frac{kd}{2}))} \sim \frac{2\chi R^3 N}{d} \sqrt{\frac{\eta\zeta}{\eta'(\eta + \zeta)^3}}. \tag{31}$$

Employing the values displayed in Table II for an EMG900 ferrofluid, we estimate the single particle velocity to be

$$\langle v_p \rangle \sim \chi 1.1 \times 10^{-3} \text{ cm/s}. \tag{32}$$

Clearly, this estimate can become larger by employing, for instance, larger chiral particles.

TABLE II. Experimental values taken from Refs. [11,17,20] for EMG 900_2 Ferrofluid.

Quantity	Value	Definition
ρ (g cm^{-3})	1.03	Density
η (g cm^{-1} s^{-1})	0.045	Shear viscosity Eq. (3)
ζ (g cm^{-1} s^{-1})	0.003	Vortex viscosity Eq. (3)
η' (g cm s^{-1})	10^{-7}	Spin viscosity Eq. (4)
R (cm)	2×10^{-3}	Characteristic chiral particle radius
d (cm)	0.1	Characteristic channel width
N (dyne cm^{-2})	2	Characteristic torque density
τ (dyne cm^{-2})	0.1	Characteristic surface shear stress
U (cm/s)	1	Upper wall speed in Couette flow; Sec. IV D
$n^{\text{ch}}R^3$	1	Chiral density

The chiral suspension imparts forces F on the channel walls as these are depicted in Fig. 2. From Eq. (14), we obtain

$$F \equiv \sigma_{yz}^{\text{ch}}\left(y = \pm\frac{d}{2}\right) = \mp\frac{(\eta + \zeta)\alpha n^{\text{ch}}k^2 Ndl\sinh\left(\frac{kd}{2}\right)}{4\zeta\left(-l\sinh\left(\frac{kd}{2}\right) + d\cosh\left(\frac{kd}{2}\right)\right)} \sim \chi RN\sqrt{\frac{\eta\zeta}{\eta'(\eta+\zeta)}} \sim 0.67\chi \text{ dynes cm}^{-2}.$$

(33)

The chiral stress $F = \sigma_{yz}^{\text{ch}}$ in Eq. (49) is perpendicular to the plane of the page and applies two evenly oriented forces F on the channel walls in the y direction.

For comparison with the liquid undisturbed by the presence of the chiral particles, we calculate the shear stresses $\sigma_{xz} = (\eta + \zeta)\partial_z u - 2\zeta\omega$ and $\sigma_{zx} = (\eta - \zeta)\partial_z u + 2\zeta\omega$, and average over the channel width to obtain

$$\langle\sigma_{zx}\rangle = -\langle\sigma_{xz}\rangle = \frac{N\left(d\cosh\left(\frac{kd}{2}\right)k - 2\sinh\left(\frac{kd}{2}\right)\right)}{2k\left(-l\sinh\left(\frac{kd}{2}\right) + d\cosh\left(\frac{kd}{2}\right)\right)} \sim \frac{N}{2} = 1 \text{ dyne cm}^{-2}.$$

(34)

The order of magnitude of this estimate agrees with well-known results obtained in systems of similar size in technology and biology, cf. Ref. [21]. The opposite sign between the stresses arises due to the fact that with no-slip boundary conditions, $\langle\partial_z u\rangle = 0$ so $\langle\sigma_{zx}\rangle = -\langle\sigma_{xz}\rangle = 2\zeta\langle\omega\rangle$.

We calculate the Reynolds number with the channel width d being the characteristic length and characteristic velocity is chosen to be the two-norm of the liquid velocity, giving the approximate expression $\|u\|_2 \sim \sqrt{\frac{6\eta'}{\eta\zeta(\eta+\zeta)}}\frac{N}{24} \sim 3 \times 10^{-2}$ cm/s. Thus,

$$\text{Re} \sim 6 \times 10^{-2}.$$

(35)

The chiral stress Eq. (49) generates a chiral volume force density $-\partial_z\sigma_{yz}^{\text{ch}}$ that maintains a chiral velocity directed perpendicularly to the plane of the duct and satisfies Eqs. (23) and (24). We solve these equations numerically, subject to the material constants displayed in Table II. Averaging over the channel width leads to the estimate

$$\langle v^{\text{ch}}\rangle \sim 4\chi \times 10^{-2} \text{ cm/s}.$$

(36)

This rather large value is the largest of all chiral velocities we calculated for the cases that follow, which shows that the application of a torque is a very effective way to propel passive chiral particles and disturb the flow in a direction perpendicular to its unperturbed direction.

The chiral velocity v^{ch} [see Eq. (36)] of suspended chiral particles of density $n^{\text{ch}} = n^+ - n^-$ is directed perpendicularly to the plane of the channel: out of the page $\odot$ at the whole expanse of the channel, cf. Fig. 2.

The right panel of Fig. 2 displays the spatial distribution of the observables v_p, σ^{ch} and v^{ch}. Here we show the velocity v_p for a particle with chirality coefficient $\chi = 1$. A particle of opposite

TABLE III. Particle size and spin viscosity values for Secs. IV C–IV E.

Quantity	Value	Definition
$\eta'(\text{g cm s}^{-1})$	10^{-9}	Spin viscosity Eq. (4)
R (cm)	6×10^{-3}	Characteristic chiral particle radius

chirality will move in the opposite direction. Following the convention described in the previous section, the chiral stress and velocity are associated with a chiral current $n^{\text{ch}} > 0$.

C. Chiral particle propulsion in pressure-driven flow

In the absence of an external torque, a liquid with rotational degrees of freedom can still give rise to chiral particle propulsion by way of vorticity diffusion. In this section, we consider a constant pressure gradient $\partial_x p$ applied in a suspension of chiral particles in a liquid with rotational degrees of freedom. We employ again the boundary conditions Eqs. (42) of no slip and no-particle rotation at the channel walls $u = 0$, and $\omega = 0$ at $z = \pm\frac{d}{2}$, and substitute into Eqs. (10) and (11) to obtain the closed form expressions for the fields u and ω that appear in Appendix B.

Employing the dimensional parameters k and l (see Table I), substituting the unperturbed velocity profile $u(z) = -\frac{((d^2-4z^2)\sinh(\frac{dk}{2})+dl(e^{kz}+e^{-kz}-2\cosh(\frac{dk}{2})))\partial_x p}{8\eta\sinh(\frac{dk}{2})}$ directly into Eq. (20) and averaging its square over the channel width, we obtain the single particle velocity v_p:

$$\|v_p\|_2 \equiv \frac{\|j^{\text{ch}}\|_2}{n} = \frac{\sqrt{2}\,R^3\chi\,k^2 l\sqrt{d(-dk+\sinh(dk))k\,\partial_x p^2}}{8\eta\sinh(\frac{dk}{2})} \sim \frac{\sqrt{2}\,\sqrt{dk}\,\chi\,R^3 k^2 l\partial_x p}{8\eta}. \quad (37)$$

Employing the values displayed in Table II for an EMG900 ferrofluid, we estimate the single-particle velocity to be

$$\|v_p\|_2 \sim \chi 3 \times 10^{-2} \text{ cm/s}. \quad (38)$$

This estimate was obtained by balancing the pressure gradient with the contraction of the stress tensor $\partial_x p = \frac{\eta U}{d^2} \sim 4.5$ dynes/cm, and by employing the values from Table II. Here we also employed larger particle sizes and a smaller value for the spin viscosity η', as these are displayed in Table III.

The chiral suspension imparts forces F on the channel walls as depicted in Fig. 3. From Eq. (14), we obtain

$$F \equiv \sigma_{yz}^{\text{ch}}\left(y = \pm\frac{d}{2}\right) = -n^{\text{ch}}\alpha\frac{(ld\,k^2\cosh(\frac{dk}{2}) - 4\sinh(\frac{dk}{2}))\partial_x p}{4\eta\sinh(\frac{dk}{2})} \sim \frac{\chi R \zeta^{\frac{3}{2}} d\partial_x p}{\sqrt{\eta}\,\sqrt{\eta+\zeta}\,\sqrt{et}}$$

$$\sim 0.27\chi\,\text{dynes cm}^{-2}, \quad (39)$$

The chiral stress $F = \sigma_{yz}^{\text{ch}}$ in Eq. (49) is perpendicular to the plane of the page and applies two oppositely directed forces F in the channel walls in the y direction.

We calculate the Reynolds number with channel width d being the characteristic length and the characteristic velocity is chosen to be the two-norm of the liquid velocity, giving the approximate expression $\|u\|_2 \sim 0.09$ cm/s. Thus,

$$\text{Re} \sim 0.17. \quad (40)$$

In a base Poiseuille flow of a standard Newtonian liquid, the chiral part of the stress tensor Eq. (14) *does not* generate a volume force density $-\partial_j \sigma_{ij}^{\text{ch}}$ inside the liquid, cf. Ref. [10], and the flow is not affected by the chiral character of the suspended particles. On the other hand, in a liquid with rotational degrees of freedom, such as the one considered in the present paper, the chiral part of the stress tensor Eq. (14) *does* generate a volume force density inside the liquid. Thus, the flow here
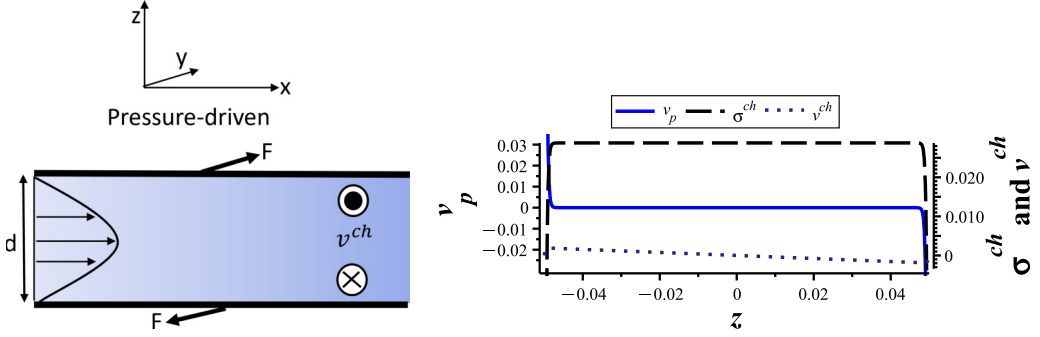
FIG. 3. Pressure-driven flow of a liquid with rotational degrees of freedom in a channel of width d whose dynamics is described by the stress and couple tensors Eqs. (3) and (4) gives rise to passive chiral particle propulsion. A chiral current $\mathbf{j}^{\text{ch}}$ [cf. Eq. (16)] is driven by the diffusion of liquid vorticity which in turn is driven by the pressure gradient and the angular velocity imbalance curl$\mathbf{u} - 2\boldsymbol{\omega}$. The single chiral particle velocity is denoted by v_p. A chiral stress $F = \sigma_{yz}^{\text{ch}}$ perpendicular to the plane of the page [see Eq. (14)] applies two oppositely directed forces F on the channel walls in the y direction. This stress also gives rise to a chiral volume force density $-\partial_z \sigma_{yz}^{\text{ch}}$ and a chiral velocity v^{ch} [see Eq. (41)] of suspended chiral particles of density $n^{\text{ch}} = n^+ - n^-$ directed perpendicularly to the plane of the channel: into the page $\otimes$ at the lower half and out-of-the-page $\odot$ at the upper half of the channel. Right panel: Spatial distribution of the observables v_p, σ^{ch} and v^{ch} in Gaussian units, setting $\chi = 1$.

is affected by the chiral character of the suspended particles. The chiral stress Eq. (49) generates a chiral volume force density $-\partial_z \sigma_{yz}^{\text{ch}}$ that maintains a chiral velocity directed perpendicularly to the plane of the duct and satisfies Eqs. (23) and (24). We solve these equations analytically, subject to the material constants displayed in Table II with η' and R taken from Table III. The average over the channel width vanishes, so we calculate the two-norm:

$$\|v^{\text{ch}}\|_2 \sim 1.1 \times 10^{-3} \chi \quad \text{cm/s}. \tag{41}$$

The chiral stress $F = \sigma_{yz}^{\text{ch}}$ in Eq. (39) is perpendicular to the plane of the page and applies two oppositely directed forces F on the channel walls in the y direction. The chiral velocity v^{ch} [see Eq. (41)] of suspended chiral particles of density $n^{\text{ch}} = n^+ - n^-$ is directed perpendicularly to the plane of the channel: into the page $\otimes$ at the lower half and out of the page $\odot$ at the upper half of the channel, cf. Fig. 3.

In the right panel of Fig. 3, we display the spatial distribution of the observables v_p, σ^{ch} and v^{ch}. The employment of a small spin viscosity value from Table III has generated sharp boundary-layer-type spatial profiles close to the rigid walls. This pattern will persist in the following two sections where this low spin viscosity value is also adopted.

D. Chiral separation in Couette flow

The practically important case of Couette flow in a liquid with rotational degrees of freedom will also give rise to vorticity diffusion-induced chiral particle propulsion. We calculate below the single particle velocity, chiral stress, and chiral velocity for a liquid suspension in a channel of width d whose upper wall moves at a constant speed U, in the absence of a torque or pressure gradient. We employ the boundary conditions of no-slip and no-particle rotation at the channel walls,

$$u = U, \quad \text{at } z = \frac{d}{2}, \quad u = 0 \quad \text{at } z = -\frac{d}{2} \quad \text{and} \quad \omega = 0, \quad \text{at } z = \pm\frac{d}{2}, \tag{42}$$

respectively, and substitute into Eqs. (10) and (11) to obtain the closed form expression for the fields u and ω that appear in Appendix B.
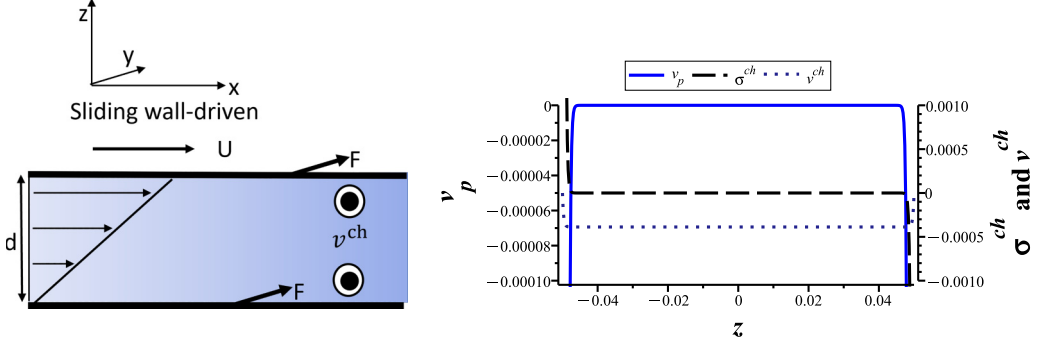
FIG. 4. Couette flow of a liquid with rotational degrees of freedom in a channel of width d whose dynamics is described by the stress and couple tensors Eqs. (3) and (4) gives rise to passive chiral particle propulsion. A chiral current $\mathbf{j}^{\text{ch}}$ [cf. Eq. (16)] is driven by the diffusion of liquid vorticity which in turn is driven by the motion of the upper wall with velocity U and the angular velocity imbalance $\text{curl}\,\mathbf{u} - 2\boldsymbol{\omega}$. The single chiral particle velocity is denoted by v_p. A chiral stress $F = \sigma_{yz}^{\text{ch}}$ perpendicular to the plane of the page [see Eq. (14)] applies two evenly directed forces F on the channel walls in the y direction. This stress also gives rise to a chiral volume force density $-\partial_z \sigma_{yz}^{\text{ch}}$ and a chiral velocity v^{ch} [see Eq. (46)] of suspended chiral particles of density $n^{\text{ch}} = n^+ - n^-$ is directed perpendicularly to the plane of the channel: out of the page $\odot$ at the whole expanse of the channel. Right panel: Spatial distribution of the observables v_p, σ^{ch} and v^{ch} in Gaussian units (the vertical range has been restricted by one order of magnitude for clarity).

Employing the dimensional parameters k and l (see Table I), substituting the unperturbed velocity profile $u(z) = \frac{((d+2z)\cosh(\frac{kd}{2}) - l(\sinh(kz) + \sinh(\frac{kd}{2})))U}{2d\cosh(\frac{kd}{2}) - 2l\sinh(\frac{kd}{2})}$ directly into the chiral current Eq. (16) and averaging over the channel width, we obtain the single particle velocity v_p:

$$\langle v_p \rangle \equiv \frac{\langle j^{\text{ch}} \rangle}{n} = -\frac{\sinh(\frac{kd}{2})\chi R^3 l U\, k^2}{d\left(d\cosh(\frac{kd}{2}) - l\sinh(\frac{kd}{2})\right)} \sim -\frac{4\chi R^3 U}{d^2}\sqrt{\frac{\eta\zeta^3}{\eta'(\eta+\zeta)^3}} \sim \chi 1 \times 10^{-3} \ \ \text{cm/s.} \tag{43}$$

The last estimate was obtained by employing the values displayed in Table II for an EMG900 ferrofluid and suspending *larger* chiral particles $R \sim 6 \times 10^{-3}$ compared to the particle size that led to the estimate Eq. (38), see Table III.

The chiral suspension imparts forces F on the channel walls as depicted in Fig. 4. From Eq. (14), we obtain

$$F \equiv \sigma_{yz}^{\text{ch}}\left(y = \pm\frac{d}{2}\right) = \mp\frac{n^{\text{ch}}\alpha(\eta+\zeta)U l k^2 \sinh(kz)}{2\left(d\cosh(\frac{kd}{2}) - l\sinh(\frac{kd}{2})\right)} \sim 2\chi\frac{R}{d}\sqrt{\frac{\eta\zeta^3}{\eta'(\eta+\zeta)^3}}U \sim 0.06\chi \ \ \text{dynes cm}^{-2}. \tag{44}$$

The chiral stress $F = \sigma_{yz}^{\text{ch}}$ in Eq. (44) is perpendicular to the plane of the page and applies two evenly directed forces F in the channel walls in the y direction.

We calculate the Reynolds number with the above values, whose characteristic velocity is chosen to be the two-norm of the unperturbed by chirality liquid velocity giving the approximate expression $\|u\|_2 \sim 0.058$ cm/s. Thus,

$$\text{Re} \sim 0.124. \tag{45}$$

As is the case in the base Poiseuille flow of a standard Newtonian liquid, the chiral part of the stress tensor Eq. (14) for the Couette *does not* generate a volume force density $-\partial_j \sigma_{ij}^{\text{ch}}$ inside the liquid, cf. Ref. [10], and the flow is not affected by the chiral character of the suspended particles. On the other hand, in a liquid with rotational degrees of freedom, such as the one considered in the present paper, the chiral part of the stress tensor Eq. (14) *does* generate a volume force density
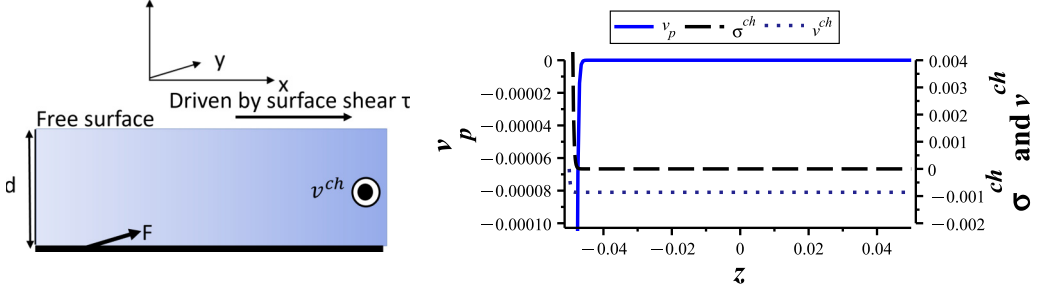
FIG. 5. Free-surface flow of a liquid layer of thickness d endowed with rotational degrees of freedom above a solid substrate and surrounded by an ambient gas phase and driven by surface shear τ gives rise to passive chiral particle propulsion. A chiral current $\mathbf{j}^{\mathrm{ch}}$ [cf. Eq. (16)] is driven by the diffusion of liquid vorticity which in turn is driven by the pressure gradient and the angular velocity imbalance curl$\mathbf{u} - 2\boldsymbol{\omega}$. The single chiral particle velocity is denoted by v_p. A chiral stress $F = \sigma_{yz}^{\mathrm{ch}}$ perpendicular to the plane of the page [see Eq. (14)] applies a force F on the lower channel walls in the y direction. This stress also gives rise to a chiral volume force density $-\partial_z \sigma_{yz}^{\mathrm{ch}}$ and a chiral velocity v^{ch} [see Eq. (51)] of suspended chiral particles of density $n^{\mathrm{ch}} = n^+ - n^-$ is directed perpendicularly to the plane of the channel: out of the page ⊙. Right panel: Spatial distribution of the observables v_p, σ^{ch} and v^{ch} in Gaussian units (the vertical range has been restricted by one order of magnitude for clarity).

inside the liquid. Thus, the flow here *is* affected by the chiral character of the suspended particles. The chiral stress Eq. (49) generates a chiral volume force density $-\partial_z \sigma_{yz}^{\mathrm{ch}}$ that maintains a chiral velocity directed perpendicularly to the plane of the duct and satisfies Eqs. (23) and (24). We solve these equations analytically, subject to the material constants displayed in Table II, with η' and R taken from Table III. The average over the channel width reads

$$\langle v^{\mathrm{ch}} \rangle \sim 4 \times 10^{-4} \chi \quad \mathrm{cm/s}. \tag{46}$$

In the right panel of Fig. 4, we display the spatial distribution of the observables v_p, σ^{ch}, and v^{ch} in Gaussian units for $\chi = 1$. The employment of a small spin viscosity value from Table III has generated sharp boundary-layer-type spatial profiles close to the rigid walls.

E. Chiral propulsion in a liquid with a flat free interface under surface shear τ

In the previous three sections, we considered a suspension of chiral particles in a liquid with rotational degrees of freedom confined within rigid walls. Diffusion of vorticity also arises, however, when a free surface is acted upon by surface shear. Here, we will consider the simplest possible case of a free surface, a flat interface between the liquid and an ambient gas phase. Thus, consider the situation displayed in Fig. 5. A constant surface shear τ is applied on the free surface of the liquid lying at $z = d/2$. The boundary conditions become [15,22]

$$u(-d/2) = 0, \quad \omega(-d/2) = 0, \quad (\eta + \zeta)\partial_z u(d/2) - 2\zeta \omega(d/2) = \tau, \quad \partial_z \omega(d/2) = 0. \tag{47}$$

Solving Eq. (10) and (11) with the above boundary conditions, substituting the unperturbed velocity profile $u(z)$ (see Appendix B) directly into the chiral current Eq. (16) (by employing the dimensional parameters k and l, cf. Table I), and averaging over the channel width we obtain the single particle velocity v_p:

$$\langle v_p \rangle \equiv \frac{\langle j^{\mathrm{ch}} \rangle}{n} \sim \frac{2\chi R^3 \tau}{d} \sqrt{\frac{\zeta^3}{\eta' \eta (\eta + \zeta)^3}} \sim \chi 1 \times 10^{-3} \quad \mathrm{cm/s}. \tag{48}$$

The last estimate was obtained by employing the values displayed in Table II for an EMG900 ferrofluid and suspending *larger* chiral particles $R \sim 6 \times 10^{-3}$ compared to the particle size that led to the estimate Eq. (38), see Table III.

The chiral suspension imparts forces F on the bottom channel wall, depicted in Fig. 5. From Eq. (14), we obtain

$$F \equiv \sigma_{yz}^{\text{ch}}\left(y = -\frac{d}{2}\right) \sim 2\chi R\sqrt{\frac{\zeta^3}{\eta'\eta(\eta + \zeta)}}\tau \sim 0.13\chi \ \text{dynes cm}^{-2}. \tag{49}$$

We calculate the Reynolds number with the above values, whose characteristic velocity is chosen to be the two-norm of the liquid velocity giving the approximate expression $\|u\|_2 \sim 0.11$ cm/s. Thus,

$$\text{Re} \sim 0.27. \tag{50}$$

To obtain expressions for the chiral velocity, we solve Eqs. (23) and (24) analytically subject to the boundary conditions Eq. (25) on the lower wall and Eqs. (26) on the free surface. Employing the material constants displayed in Table II with η' and R taken from Table III, we calculate the average over the channel width, which reads

$$\langle v^{\text{ch}} \rangle \sim 8.5 \times 10^{-4}\chi \ \text{cm/s}, \tag{51}$$

directed perpendicularly to the plane of the channel: out of the page $\odot$ cf. Fig. 5.

In the right panel of Fig. 5, we display the spatial distribution of the observables v_p, σ^{ch} and v^{ch}. The employment of a small spin viscosity value from Table III has generated sharp boundary-layer-type spatial profiles close to the lower rigid wall.

V. DISCUSSION

In this paper, we show that in a liquid with rotational degrees of freedom, suspended chiral particles can be propelled even in Stokes flow. Three mechanisms generate a spatially dependent vorticity distribution in this base liquid contained in a channel: an external magnetic field, a pressure gradient, and a sliding channel wall. When one channel wall is replaced by a free surface then the vorticity distribution is generated by a surface shear wind. These mechanisms impart energy into the base liquid and modify its internal angular momentum, creating and maintaining regions of spatially inhomogeneous vorticity. Suspending n^- left- and n^+ right-handed chiral particles on this base liquid leads to their propulsion and separation. This is because the spatially inhomogeneous vorticity is maintained by the internal angular momentum the external stimuli impart on the liquid. The chiral particle inherent shape asymmetry leads them to propel in a direction perpendicular to the plane of the vortex as is evident in the foregoing analysis summarized in Figs. 2–5. In each case, the chiral particles impart a chiral stress on the walls of the channel or substrate that are perpendicular to the flow. This effect is in contrast to its standard Newtonian liquid counterpart, where vorticity gradient-induced propulsion is impossible in Stokes flow [10].

From the right panels of Figs. 2–5, we conclude that most of the diffusion of vorticity generation and thus chiral particle propulsion takes place close to the solid walls of the channel or the free surface. This observation could be associated with the tendency of cells to swim close to surfaces, see Ref. [23], Chap. 11] and references therein.

Propulsion in noncentrosymmetric media was theoretically developed in the past for the case of photoinduced separation of chiral isomers [24], the photogalvanic effect [25], and the electron moment-induced propulsion of chiral particles [8]. The common thread in all these works is to take advantage of the transformation properties of the current under spatial inversion. The current is a polar vector and thus changes sign under spatial inversion. The current is so chosen as to be proportional to vectors or vector products that are *invariant* under spatial inversion. Thus, these effects exist only when the coefficient of proportionality changes sign under spatial inversion. In the case developed in the present paper, the effect of this sign change is that particles of opposite chirality will move in opposite directions. This principle is well-known in the area of noncentrosymmetric media [26].

These ideas also carry over to the stress tensor. In a nonracemic mixture, the chiral suspension will apply stresses on the liquid and these will be represented by a chiral stress tensor. By symmetry, it will be proportional to quantities that change signs under spatial inversion. Thus, such contributions exist only when the proportionality constant also changes signs, since the stress tensor is invariant under such a transformation.

In this paper, we chose for spin viscosity η' the value $\sim 10^{-7}$ g cm s^{-1} adopted from the experiments of Chaves *et al.* [11]. An even larger value was measured in other experiments based on a cobalt ferrite water-based ferrofluid [27]. Both disagree with theoretical estimates of this parameter (see, e.g., Ref. [28]) which show a value that is orders of magnitude smaller than the one employed here. In the same vein, comparison with equilibrium molecular dynamics simulations of water show a spin viscosity coefficient to be even smaller ($\sim 10^{-21}$ g cm s^{-1}) [29]. Of course, these are different liquids but it is good to keep in mind that the determination of the spin viscosity coefficient is still an open area of research (see the discussion in Ref. [15], Sec. IV). Thus, in Secs. IV C–IV E, we adopted the smaller value $\sim 10^{-9}$ g cm s^{-1}, merely as convenient means to reproduce chiral particle velocities of the same order of magnitude in all four cases considered here. Adopting the experimentally verified value of Chaves *et al.* [11] for Secs. IV D and IV E would give rise to very small particle velocity estimates.

In relation to the problem analyzed in Sec. IV B, an additional effect that may arise concerns the state of broken time-reversal symmetry and parity when the rotational degrees of freedom of the base liquid are driven by the magnetic field. In such a case, additional effects may arise, as was recently shown experimentally by colleagues at the University of Chicago [30]. In two dimensions, these effects are associated with the presence of an additional viscosity coefficient of the base liquid and in an incompressible liquid become prominent when boundary conditions are (partly) determined by mechanisms active at an interface (surface tension, surface shear, etc.), see, for instance, Ref. [31]. The case we consider in Sec. IV B employs the same antisymmetric tensors as Ref. [30], and is also effectively two-dimensional but lacks a free surface. As such, any effects of odd viscosity will just renormalize the state of pressure (cf. Ref. [31]) at the base flow. Were we to consider a fully three-dimensional case, effects of odd viscosity could become prominent; see, for instance, the discussion in Ref. [32] and references therein.

In this paper, we attempted to provide a logical and consistent interpretation of the chiral particle propulsion effect that was first published in Ref. [10], and extended it to the case of liquids endowed with rotational degrees of freedom incorporating couple stresses [the tensor in Eq. (4)]. In its absence (setting $\eta' \equiv 0$), the problem changes character since not all boundary conditions can be satisfied. This is a singular perturbation problem and the solution obtained without rescaling corresponds to the outer expansion [33]. Related is the form of the chiral current that is directly given by the difference between vorticity and twice the angular velocity of the rotational degrees of freedom of the base liquid: $\mathbf{j}^{\text{ch}} \sim \text{curl}\,\mathbf{u} - 2\boldsymbol{\omega}$. This alternative viewpoint will be explored in a separate publication.

The concept developed in the present paper can be applied to separate particles according to their handedness. It can also be considered as a strategy of locomotion in Stokes flow. In this sense, we believe it describes an alternative mechanism for the delivery of drugs through the bloodstream [3] and for targeting malignant cells. The latter would be an especially important application in light of recent research which shows that only 1% of particles reach their target [34].

referees for valuable comments and criticism that improved the paper, and for bringing a number of references to their attention.

APPENDIX A

The Maxwell's equations are $\nabla \times \mathbf{h} = \mathbf{0}$ and $\nabla \cdot \mathbf{b} = 0$, where $\mathbf{b} = \mathbf{h} + 4\pi \mathbf{m}$ with $\mathbf{m}$ being the macroscopic magnetization of the base liquid. Since the torque density $\mathbf{N} = \mathbf{m} \times \mathbf{h}$ depends on the macroscopic magnetization field $\mathbf{m}$, one more constitutive equation describing the evolution of this field has to be imposed to provide closure [11]. This is

$$Dm_i/Dt = \epsilon_{ijk}\omega_j m_k - (m_i - \xi h_i)/\tau_B \quad i = 1, 2, 3. \tag{A1}$$

Here, τ_B is the Brownian relaxation time [11], pp. 54–57 and ξ is the effective magnetic susceptibility,

$$\xi = n_g m_d L(\alpha)/h, \quad L = \coth\alpha - \frac{1}{\alpha}, \quad \alpha = \frac{m_d h}{k_B T}, \tag{A2}$$

where $m_d = M_d V$ is the magnetic moment of a single subdomain particle, V is the particle volume, M_d is the domain magnetization of dispersed ferromagnetic material, and n_g is the number density of the magnetic grains. In this form, Eq. (A1) applies only at moderate strengths of the applied field. For a discussion of this point, see Ref. [11], pp. 54–57 and references therein.

APPENDIX B

Below we solve the equations of motion Eqs. (10) and (11) for a fluid in a channel with constant torque N [17] and constant pressure gradient $\partial_x p$,

$$\omega = \frac{z\partial_x p}{2\eta} + A + Be^{-kz} + Ce^{kz} + \frac{N}{4\zeta}, \tag{B1}$$

$$u = \frac{z^2\partial_x p}{2\eta} + 2Az - l(Be^{-kz} - Ce^{kz}) + D, \tag{B2}$$

$$(\text{curl}\mathbf{u})_y = \frac{z\partial_x p}{\eta} + 2A + kl(Be^{-kz} + Ce^{kz}), \tag{B3}$$

where $l = \sqrt{\frac{\zeta\eta'}{\eta(\eta+\zeta)}}$ and $k = \sqrt{\frac{4\eta\zeta}{\eta'(\eta+\zeta)}}$ and $A, B, C,$ and D are arbitrary constants determined by the boundary conditions. For a channel of width d, they are $u(\pm d/2) = \omega(\pm d/2) = 0$, adapted from Refs. [11,17]. When the upper wall moves with speed U, one of them is replaced by $u(d/2) = U$. N is the (constant) torque and $\partial_x p$ the pressure gradient:

$$A = \frac{Nl\sinh\left(\frac{kd}{2}\right) + 2U\zeta\cosh\left(\frac{kd}{2}\right)}{4\zeta\left(-l\sinh\left(\frac{kd}{2}\right) + d\cosh\left(\frac{kd}{2}\right)\right)}, \tag{B4}$$

$$B = \frac{((\partial_x p d l + 2U\eta)\zeta + Nd\eta)\sinh\left(\frac{kd}{2}\right) - d^2\partial_x p\zeta\cosh\left(\frac{kd}{2}\right)}{8\eta\zeta\left(l\sinh\left(\frac{kd}{2}\right) - d\cosh\left(\frac{kd}{2}\right)\right)\sinh\left(\frac{kd}{2}\right)}, \tag{B5}$$

$$C = \frac{((-\partial_x p d l + 2U\eta)\zeta + Nd\eta)\sinh\left(\frac{kd}{2}\right) + d^2\partial_x p\zeta\cosh\left(\frac{kd}{2}\right)}{8\eta\zeta\left(l\sinh\left(\frac{kd}{2}\right) - d\cosh\left(\frac{kd}{2}\right)\right)\sinh\left(\frac{kd}{2}\right)}, \tag{B6}$$

$$D = \frac{2\partial_x p d l\cosh\left(\frac{kd}{2}\right) - d^2\partial_x p\sinh\left(\frac{kd}{2}\right) + 4U\eta\sinh\left(\frac{kd}{2}\right)}{8\eta\sinh\left(\frac{kd}{2}\right)}. \tag{B7}$$

Below we solve the equations of motion (10) and (11) for a fluid layer (hard wall at $y = -d/2$ and free surface at $y = d/2$) in the absence of both torque and pressure gradient. In this case, the liquid is forced by a constant surface shear τ. Thus, the boundary conditions become (cf. Ref. [15]),

$$u(-d/2) = 0, \quad \omega(-d/2) = 0, \quad (\eta + \zeta)\partial_z u(d/2) - 2\zeta\omega(d/2) = \tau, \quad \partial_z\omega(d/2) = 0, \tag{B8}$$

giving rise to

$$A = \frac{\tau}{2\eta}, \tag{B9}$$

$$B = -\frac{\tau\left(\cosh\left(\frac{3kd}{2}\right) + \sinh\left(\frac{3kd}{2}\right)\right)}{2\eta(\cosh(2kd) + \sinh(2kd) + 1)}, \tag{B10}$$

$$C = -\frac{\tau\left(\cosh\left(\frac{3kd}{2}\right) + \sinh\left(\frac{3kd}{2}\right)\right)}{2\eta(\cosh(2kd) + \sinh(2kd) + 1)}, \tag{B11}$$

$$D = \frac{\tau(\cosh(2kd)d - l\cosh(2kd) + \sinh(2kd)d - l\sinh(2kd) + d + l)}{2\eta(\cosh(2kd) + \sinh(2kd) + 1)}. \tag{B12}$$

[1] M. C. Marchetti, J.-F. Joanny, S. Ramaswamy, T. B. Liverpool, J. Prost, M. Rao, and R. A. Simha, Hydrodynamics of soft active matter, Rev. Mod. Phys. **85**, 1143 (2013); M. Driscoll and B. Delmotte, Leveraging collective effects in externally driven colloidal suspensions: Experiments and simulations, Curr. Opin. Colloid Interface Sci. **40**, 42 (2019).

[2] M. E. Cates and J. Tailleur, Motility-induced phase separation, Annu. Rev. Condens. Matter Phys. **6**, 219 (2015).

[3] B. Zhang, H. Yuan, A. Sokolov, M. Olvera de la Cruz, and A. Snezhko, Polar state reversal in active fluids, Nat. Phys. **18**, 154 (2022); I. Torres-Díaz and C. Rinaldi, Recent progress in ferrofluids research: Novel applications of magnetically controllable and tunable fluids, Soft Matter **10**, 8584 (2014).

[4] J. Palacci, S. Sacanna, A. P. Steinberg, D. J. Pine, and P. M. Chaikin, Living crystals of light-activated colloidal surfers, Science **339**, 936 (2013); J. Zhang, R. Alert, J. Yan, N. S. Wingreen, and S. Granick, Active phase separation by turning towards regions of higher density, Nat. Phys. **17**, 961 (2021).

[5] A. M. Brooks, M. Tasinkevych, S. Sabrina, D. Velegol, A. Sen, and K. J. M. Bishop, Shape-directed rotation of homogeneous micromotors via catalytic self-electrophoresis, Nat. Commun. **10**, 1 (2019).

[6] W. A. Bonner, The origin and amplification of biomolecular chirality, Origins of Life and Evol. Biosphere **21**, 59 (1991).

[7] T. A. Witten and H. Diamant, A review of shaped colloidal particles in fluids: Anisotropy and chirality, Rep. Prog. Phys. **83**, 116601 (2020).

[8] E. Kirkinis, A. V. Andreev, and B. Spivak, Electromagnetic propulsion and separation by chirality of nanoparticles in liquids, Phys. Rev. E **85**, 016321 (2012); M. Doi and M. Makino, Separation of chiral particles in a rotating electric field, Phys. Fluids **28**, 093302 (2016); M. Makino and M. Doi, Separation of propeller-like particles by shear and electric field, Phys. Rev. Fluids **2**, 064303 (2017).

[9] M. Makino and M. Doi, Migration of twisted ribbon-like particles in simple shear flow, Phys. Fluids **17**, 103605 (2005); S. Meinhardt, J. Smiatek, R. Eichhorn, and F. Schmid, Separation of Chiral Particles in Micro-or Nanofluidic Channels, Phys. Rev. Lett. **108**, 214504 (2012).

[10] A. V. Andreev, D. T. Son, and B. Spivak, Hydrodynamics of Liquids of Chiral Molecules and Suspensions Containing Chiral Particles, Phys. Rev. Lett. **104**, 198301 (2010).

[11] C. Rinaldi, Continuum modeling of polarizable systems, Ph.D. thesis, Massachusetts Institute of Technology, 2002; A. Chaves, M. Zahn, and C. Rinaldi, Spin-up flow of ferrofluids: Asymptotic theory and experimental measurements, Phys. Fluids **20**, 053102 (2008).

[12] J. S. Dahler and L. E. Scriven, Angular momentum of continua, Nature **192**, 36 (1961); D. W. Condiff and J. S. Dahler, Fluid mechanical aspects of antisymmetric stress, Phys. Fluids **7**, 842 (1964); E. L. Aero, A. N. Bulygin, and E. V. Kuvshinskii, Asymmetric hydromechanics, J. Appl. Math. Mech. **29**, 333 (1965).

[13] E. Kirkinis and S. H. Davis, Hydrodynamic Theory of Liquid Slippage on a Solid Substrate Near a Moving Contact Line, Phys. Rev. Lett. **110**, 234503 (2013); Moffatt vortices induced by the motion of a contact line, J. Fluid Mech. **746**, R3 (2014).

[14] M. J. Davis, M. B. Gratton, and S. H. Davis, Suppressing van der Waals driven rupture through shear, J. Fluid Mech. **661**, 522 (2010); E. Kirkinis and S. H. Davis, Stabilization mechanisms in the evolution of thin liquid-films, Proc. R. Soc. London A **471**, 20150651 (2015).

[15] A. Chaves and C. Rinaldi, Interfacial stress balances in structured continua and free surface flows in ferrofluids, Phys. Fluids **26**, 042101 (2014).

[16] A. Aggarwal, E. Kirkinis, and M. Olvera de la Cruz, Activity-induced migration of viscous droplets on a solid substrate, J. Fluid Mech. **955**, A10 (2023).

[17] M. Zahn and P. N. Wainman, Effects of fluid convection and particle spin on ferrohydrodynamic pumping in traveling wave magnetic fields, J. Magn. Magn. Mater. **122**, 323 (1993); M. Zahn and D. R. Greer, Ferrohydrodynamic pumping in spatially uniform sinusoidally time-varying magnetic fields, *ibid.* **149**, 165 (1995); A. Chaves, C. Rinaldi, S. Elborai, X. He, and M. Zahn, Bulk Flow in Ferrofluids in a Uniform Rotating Magnetic Field, Phys. Rev. Lett. **96**, 194501 (2006).

[18] L. D. Landau and E. M. Lifshitz, *Fluid Mechanics*, Course of Theoretical Physics, Vol. 6 (Pergamon Press Ltd., London, 1987).

[19] J. Happel and H. Brenner, *Low Reynolds Number Hydrodynamics with Special Applications to Particulate Media* (Prentice-Hall Inc., Englewood Cliffs, NJ, 1965).

[20] C. Rinaldi and M. Zahn, Effects of spin viscosity on ferrofluid flow profiles in alternating and rotating magnetic fields, Phys. Fluids **14**, 2847 (2002).

[21] D. E. Kataoka and S. M. Troian, Patterning liquid flow on the microscopic scale, Nature **402**, 794 (1999); J. Ando and K. Yamamoto, Vascular mechanobiology endothelial cell responses to fluid shear stress, Circ. J. **73**, 1983 (2009).

[22] E. Kirkinis, Magnetic torque-induced suppression of van-der-Waals-driven thin liquid film rupture, J. Fluid Mech. **813**, 991 (2017).

[23] E. Lauga, *The Fluid Dynamics of Cell Motility*, Cambridge Texts in Applied Mathematics (Cambridge University Press, Cambridge, 2020).

[24] B. Spivak and A. V. Andreev, Photoinduced Separation of Chiral Isomers in a Classical Buffer Gas, Phys. Rev. Lett. **102**, 063004 (2009).

[25] E. Deyo, L. E. Golub, E. L. Ivchenko, and B. Spivak, Semiclassical theory of the photogalvanic effect in non-centrosymmetric systems, arXiv:0904.1917.

[26] B. I. Sturman and V. M. Fridkin, *The Photovoltaic and Photorefractive Effects in Noncentrosymmetric Materials* (Routledge, London, 2021).

[27] I. Torres-Diaz, A. Cortes, Y. Cedeño-Mattei, O. Perales-Perez, and C. Rinaldi, Flows and torques in Brownian ferrofluids subjected to rotating uniform magnetic fields in a cylindrical and annular geometry, Phys. Fluids **26**, 012004 (2014).

[28] S. Feng, A. L. Graham, J. R. Abbott, and H. Brenner, Antisymmetric stresses in suspensions: Vortex viscosity and energy dissipation, J. Fluid Mech. **563**, 97 (2006).

[29] J. S. Hansen, H. Bruus, B. D. Todd, and P. J. Daivis, Rotational and spin viscosities of water: Application to nanofluidics, J. Chem. Phys. **133**, 144906 (2010).

[30] V. Soni, E. S. Bililign, S. Magkiriadou, S. Sacanna, D. Bartolo, M. J. Shelley, and W. T. M. Irvine, The odd free surface flows of a colloidal chiral fluid, Nat. Phys. **15**, 1188 (2019).

[31] E. Kirkinis, J. Mason, and M. Olvera de la Cruz, Odd viscosity-induced passivation of Moffatt vortices, J. Fluid Mech. **950**, A19 (2022); E. Kirkinis, Null-divergence nature of the odd viscous stress for an incompressible liquid, Phys. Rev. Fluids **8**, 014104 (2023).

[32] T. Khain, C. Scheibner, M. Fruchart, and V. Vitelli, Stokes flows in three-dimensional fluids with odd and parity-violating viscosities, J. Fluid Mech. **934**, A23 (2022).

[33] R. E. O'Malley, Jr. and E. Kirkinis, Examples illustrating the use of renormalization techniques for singularly perturbed differential equations, Stud. Appl. Math. **122**, 105 (2009); A combined renormalization group-multiple scale method for singularly perturbed problems, **124**, 383 (2010).

[34] S. Wilhelm, A. J. Tavares, Q. Dai, S. Ohta, J. Audet, H. F. Dvorak, and W. C. W. Chan, Analysis of nanoparticle delivery to tumours, Nat. Rev. Mater. **1**, 16014 (2016).